Available online at www.sciencedirect.com
SCIENCE DIRECT®
ELSEVIER
Nuclear Instruments and Methods in Physics Research A 531 (2004) 544–559
NUCLEAR INSTRUMENTS & METHODS IN PHYSICS RESEARCH Section A
www.elsevier.com/locate/nima

Efficiency at different interaction depths in large coplanar CdZnTe detectors

R. González[a], J.M. Pérez[a,*], Z. He[b]

[a] Laboratorio General de Electrónica y Automática, CIEMAT, Avda Complutense, Edificio 22, E-28040 Madrid, Spain
[b] Department of Nuclear Engineering and Radiological Sciences, The University of Michigan, Ann Arbor, MI, USA

Received 19 December 2003; received in revised form 26 April 2004; accepted 2 May 2004

Available online 19 June 2004

Abstract

This paper presents some studies performed with a state of the art large volume, 1.5 cm diameter × 1.0 cm thick, cylindrical CdZnTe coplanar detector with a new anode pattern design in the line of units previously reported. The absolute efficiency of the detector for different interaction depths is quantified. The detector's ideal response is simulated with a Monte Carlo code and compared with experimental results. Some conclusions regarding interaction depth profiles, detector efficiency, the new anode pattern design and device quality are reported. These are further compared with the behavior of previous coplanar units.

PACS: 29.40.Wk; 72.80.Ey; 73.40.Rw; 73.40.Sx

Keywords: CdZnTe; CZT; Gamma detectors; Coplanar; Simulation; Monte Carlo; Detector efficiency

1. Introduction

The extensive work performed on CZT detectors both in research laboratories and industry has led to the development of devices with volumes that would have been unimaginable some years ago. However, recent studies [1–3] show that CZT detectors, with a volume larger than 1 cm^3 and an energy resolution below 3% FWHM for ^{137}Cs, can now have practical applications. This new development was made possible with improvements in large volume crystal growth and surface treatment techniques. Other important developments that have helped the advancement of large volume detectors are the new concepts in electrode design, such as coplanar grids [4,5], and pixel arrays. These large volume CZT detectors have definitively demonstrated that room temperature semiconductor detectors are becoming a true alternative to classical cryogenic Ge detectors.

It is well known that to provide high resolution with current thick CZT detectors electron trapping correction must be applied on the difference anode signal. This can be achieved by using different

*Corresponding author. Tel.: +34-91-346-6557; fax: +34-91-346-6275.
E-mail address: jm.perez@ciemat.es (J.M. Pérez).

0168-9002/$ - see front matter © 2004 Elsevier B.V. All rights reserved.
doi:10.1016/j.nima.2004.05.081

methods, such as the analog differential anode gain approach [5] or by estimating the photon interaction depth. In coplanar detectors, as previously reported [6], differences in spectrometric capabilities at different interaction depths are related to the anode pattern design, particularly on non-symmetries in the weighting potentials associated with each anode. On the other hand, the study of the efficiency profile at different depths can provide information about possible undesired effects within the detector.

In this paper we present a work performed with a new coplanar electrode design, labeled as generation IV, as the next generation from previous designs [7]. The work in this paper involves both experimental studies and Monte Carlo simulations, and is basically focused on the comparison of the expected and experimental detector efficiency at different depths. We will show the performance of this electrode design, and compare it with designs previously reported. Discrepancies between experimental and simulated results in the resolution of the method used for depth sensing are presented here, together with a discussion on the possible effects of the hole transport in the interaction depth estimate.

In spite of the good results shown by the electrode design or electron trapping in the unit we studied, its overall spectrometric performance is poorer than expected. We have, however, brought to light some possible causes for this limitation.

2. Setup

2.1. Detector

The detector presented in this paper, M02.2-1 manufactured by eV Products, is a 1.0 cm thick CZT cylindrical detector, 1.5 cm diameter, with a coplanar anode pattern on one face and a planar cathode on the opposite face. The anode pattern (Fig. 1) was designed in order to balance, as much as possible, the two anode weighting potentials. A guard ring in the peripheral region reduces the surface leakage current to the anode face. The anode strips and the gap in the central region are

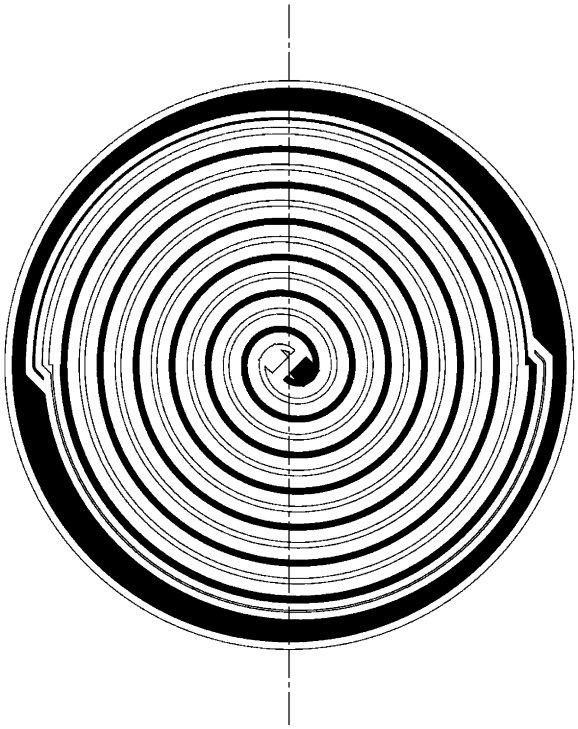

Fig. 1. Schematic representation of the M02.2-1 detector anode pattern.

0.150 and 0.325 mm wide, respectively. The outermost ring of each anode spiral has different width values: the half ring closer to the guard ring (top half in the anode in black on Fig. 1) is 0.050 mm wide, the other half is 0.175 mm. The gap surrounding this last anode ring is 0.200 mm wide.

A 3D electrostatic field calculation program was used to compute the weighting potentials associated with the anodes in the bulk, in a similar way as was carried out in Ref. [6]. Since anode weighting potentials tend to be identical in the cathode face and completely different in anode face, we present results obtained at a depth of 1 mm below the anode surface. This depth is representative for checking maximum effective differences in the weighting potentials throughout the whole bulk. Fig. 2a shows the calculated weighting potential values for the two anodes in the vertical axis of the pattern shown in Fig. 1 at a depth of 1 mm below the anode surface. Fig. 2b shows a detailed view of the relative differences, an

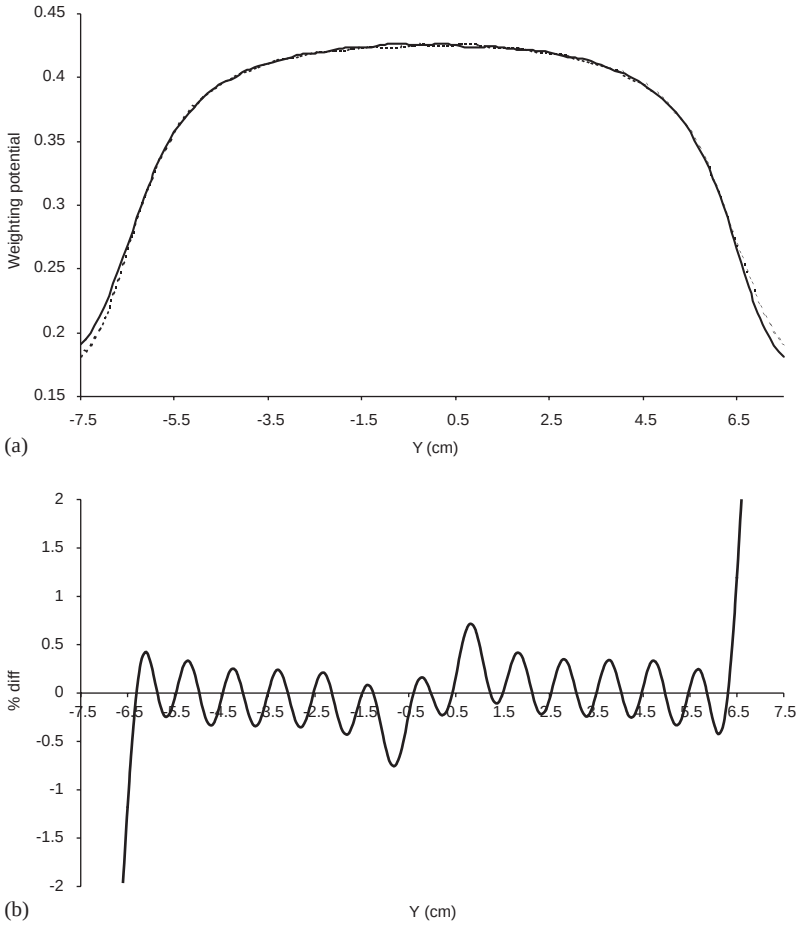

Fig. 2. (a) Weighting potentials (in dimensionless units) of the two coplanar anodes computed for the anode pattern in the coplanar detector at 1 mm depth below the anode surface, in the dashed vertical line represented in Fig. 1. (b) Relative differences of weighting potentials shown in part (a).

indication of the quality of anode pattern design. It must be pointed out that relative differences rise to 8% in the region close to the pads at the center of the detector and this is due to the loss of symmetry.

2.2. Nuclear electronics

The analog nuclear electronics setup used in this study is the conventional one used for coplanar detectors. The induced charge pulses in the anodes are read out by two AC coupled A250 preamplifiers (Amptek), mounted on PCA250 circuit boards. The output of the preamplifiers are connected to a subtraction circuit, with a relative gain that can be adjusted to correct for electron trapping [5]. The subtraction circuit is based on three AD829 (Analog Devices) operational amplifiers, mounted on a custom board. In order to obtain information regarding the photon interaction depth, the cathode signal is read out by a third preamplifier mounted in AC configuration. Our detector setup, therefore, delivers four output signals: collecting anode direct output, non-collecting anode direct output, subtracted anodes signal and cathode output. Nominal biases are

−1600 V at cathode, −60 V at non-collecting anode and 0 V at collecting anode (guard ring grounded).

The subtraction circuit output is followed by a gaussian shaper amplifier in order to enhance the signal to noise ratio, using a shaping time long enough to fully collect the induced electron charge. We have used an Ortec 855 module, with 2 μs shaping time. Its output is processed by an Aptec series 5000 multichannel analyzer. The subtraction circuit gain is adjusted in order to reach the best possible spectrometric resolution in the 662 keV photopeak of a ^{137}Cs calibration radioactive source.

The interaction depth in coplanar detectors can be estimated by combining the signals from cathode and anodes. As explained in detail in Ref. [7], the difference of the two anode pulses generated by the interaction of an incoming photon is practically insensitive to the hole transport in the bulk. The dependence on the interaction depth of the difference of the charge induced in the anodes is mainly related to electron trapping and relative differences in the weighting potentials associated with the anodes throughout the crystal. This last effect becomes more evident towards the anode face, whilst negligible for interactions near the cathode. The anode signal in coplanar electrodes is therefore proportional to the deposited energy, with deviations ~10%. Due to the relative important hole trapping in CZT, the amplitude of cathode signal filtered with a gaussian shaper is mostly dependent on the electron drift if the shaping time is small compared with hole trapping times. The total induced charge in the cathode is linearly dependent on the electron drift time. The ratio of the amplitude of the cathode and the difference of anodes signals will therefore be proportional to the interaction depth. In practice, however, the hole contribution in the cathode signal can be a source of non-linearity in the estimate of the interaction depth and therefore affects its normalization.

In large volume detectors and photon energies around 600 keV, events with multiple interaction are much more probable than single interactions. In those events when the photon deposits its energy in more than one location in the crystal, the ratio between cathode and anode amplitudes will provide an averaged value of the interaction depth. This is weighted by the energy deposited on each individual location. For example, if a 600 keV photon deposits 200 keV in the cathode side (interaction depth = 1.0) and 400 keV in the center of the detector (interaction depth = 0.5), the ratio between cathode and anode amplitudes will provide a value for the interaction depth close to $(200 \times 1.0 + 400 \times 0.5)/600 = 0.67$.

The principle described above for estimating the interaction depth was implemented by using a digitizing system based on two Gage CompuScope 12100 PCI boards (four 12 bits digitations channels at 50 MS/s sampling rate) and a program developed in Labwindows (National Instruments). The anode signal subtraction circuit relative gain was set to 1 (no electron trapping correction). This signal and the cathode preamplifier output are read out by two gaussian shaper amplifiers with identical gain and shaping time (2 μs). The output of the shaper amplifiers are connected to the digitizers which receive anode and cathode pulses in coincidence, compute the pulse heights and their ratio then provide the depth coefficient. A total of 20 histograms are accumulated for different values of the depth coefficient. The anodes pulse amplitude is represented as a count in the corresponding energy bin of the histogram related to its estimated interaction depth. Depth coefficient 0.0 corresponds to anode side, 1.0 correspond to cathode side. Fifteen slides are considered between these two limits. Apart from these depth values, unexpected negative values or greater than 1.0 were obtained. These are due to experimental factors such as small differences in the anodes and cathode gains, interactions on detector regions where the coplanar collection does not work properly or marginal effects of holes. All unexpected-like pulses were accumulated in specific depth channels.

2.3. Monte Carlo simulation

The comparison of absolute detector efficiency in different regions of the sensitive volume with that expected in an ideal device can provide some information relating to the detector performance.

A Monte Carlo code which we presented in Ref. [2] was used to study the detector efficiency in different slides of an ideal detector. The simulation program is based on Geant4 [8], version 4.5.0. Photon and electron standard interaction processes were replaced by their low-energy versions included in the low-energy electromagnetic processes package (G4EMLOW1.1). The code was run on a personal computer using Linux Red Hat 8.3. A set of custom Monte Carlo routines were used to adapt the Geant code for gamma spectrometry studies. The simulation models a radioactive source, defined by its activity, shape and isotopic composition, irradiating a detector surrounded by electronic components and shielding materials.

A basic model for the amplitude of the charge pulses induced by the interaction of photons in the crystal is considered in the simulation. The first information stored for each interaction is the response of an ideal detector only affected by a gaussian noise contribution. The total amplitude acquired for each single event is just the total energy deposited in the sensitive region of the crystal, with a random distortion in the pulse amplitude generated assuming a Gaussian distribution, in which the parameter σ is known from the measured FWHM in the experimental spectra.

In order to check the depth sensing capability of the coplanar detector, the maximum amplitude of the pulses induced by the cathode and the anodes (collecting anode pulse amplitude minus non-collecting anode pulse amplitude) is also provided. This agrees with the models provided by the Shockley–Ramo theorem [9] for ideal coplanar devices. Effects related to the differences in the anode weighting potentials near the anode face were disregarded. The rapid rise of the induced charge in this region is supposed to occur as a step, assuming the following simple models for the total induced charge pulse amplitude:

(i) No hole contribution. In this approach, the effect of holes was disregarded. For each multiple event i in which the energy was deposited in j locations of the crystal, the amplitude computed for the anode (collecting minus non-collecting) and cathode signals are, respectively

$$E_{\mathrm{anode},i} = \sum_j (1 - e_{\mathrm{trap}} z_{ij}/L) E_{i,j}, \quad (1)$$

$$E_{\mathrm{cathode},i} = \sum_j (1 - e_{\mathrm{trap}})(z_{ij}/L) E_{i,j} \quad (2)$$

where e_{trap} is the proportion of electrons trapped per unit length (1 cm) at the working bias, z_{ij} is the depth, relative to the anode surface, of the interaction j in event i (1.0 for interactions in the cathode face, 0.0 for interactions in the anode), E_{ij} is the deposited energy of the photon at event i in the interaction j and L is the detector thickness (1 cm). In this approach, the amplitude of the cathode signal is supposed to be proportional to the interaction depth, corrected by the electron trapping in the charge drift to the anode face. In the case of the anode signal, the maximum computed amplitude does not depend on the interaction depth, except for a small proportion linearly ranging from 0.0 for interactions in the anode face up to e_{trap} for interactions in the cathode face. It must be pointed out that Eqs. (1) and (2) correspond to a linear simplification of a Hetch approach for the induced charge. This simplification introduces a source of error in the simulation that can be significant for the cases in which $z_{ij} \sim \mu\tau E$ (in our case, this quantity is larger than 1.5–2 cm).

(ii) Hole contribution. In the case of the hole contribution, the following assumptions are considered. Both collecting and non-collecting anode signals are affected by the same hole contribution. Thus, the difference of these two signals are not sensitive to hole drift and Eq. (1) holds. This simplification is valid for most of the crystal volume. It should not work in the region near the anode surface in which the electric field makes the holes drift towards the non-collecting anode instead of the cathode. This region was assumed to be negligible.

When holes are supposed to drift towards the cathode, the cathode signal is affected by this drift. We assumed that holes can drift during a time not larger than a fixed limit: $t_{\mathrm{h\_max}}$, no matter what the

interaction depth is. This is a realistic assumption, based on the charge collection method, when a gaussian amplifier is used with the shaping time shorter than the (expected) maximum hole drift time. As a consequence of the foregoing, the amplitude of the cathode signal is given by

$$h_{\text{contrib\_}ij} = \begin{cases} (1-h_{\text{trap}})((L-z_{ij})/L)E_{i,j}, & t_{\text{h}} < t_{\text{h\_max}}, \\ (t_{\text{h\_max}}\mu_{\text{h}}E/L)E_{i,j}, & t_{\text{h}} \geqslant t_{\text{h\_max}}, \end{cases} \quad (3)$$

$$E_{\text{cathode},i} = \sum_j (1-e_{\text{trap}})(z_j/L) \times E_{i,j} + h_{\text{contrib\_}ij} \quad (4)$$

where h_{trap} is the proportion of holes trapped per unit length and E is the electric field in the bulk ($-1600\,\text{V cm}^{-1}$). The same applies here as for point i; Eqs. (3) and (4) above correspond to linear simplification.

3. General results

3.1. Calibration of digitizers

Our aim was to quantify the detector response at different interaction depths. For this purpose, the response of a multiparametric multichannel analyzer (MPMCA) mounted with the digitizer boards was contrasted with that provided by a standard multichannel analyzer (MCA). A calibrated ^{137}Cs point source with activity 29,800 Bq ± 6% was located at 27 mm from the top face of detector ceramic layer support (cathode face). Some reference spectra were acquired with the MCA. In one case, the anode relative gain was adjusted to the highest possible resolution. In an other case, identical anode gains were selected, thus having spectra with poor resolution because no correction for electron trapping was performed. In both cases, the preamplifier output was filtered with a 2 μs shaping time gaussian amplifier.

The MPMCA was tested using the same radiation source–detector geometry. Two channels were active, at a sampling rate of 50 MS/s, one for the anode signal, the second for the cathode signal. The relative anode gain in the subtraction circuit was adjusted by making use of test pulser. Identical gains were considered for both anodes and were only affected by the uncertainties in the values of the 2 pF capacitor in the preamplifiers test channel. The output of the subtraction circuit was filtered by a gaussian shaper amplifier. The cathode signal gain was adjusted in the shaper module, with an identical gain as the anode channel. Digitizers were programmed to acquire coincident pulses, triggered by a threshold with the anode signal. Once a pulse was detected in the anode channel, the base line height was computed by using the initial part of the waveform (pre-trigger) and the maximum of the pulse was calculated relative to the base line. Identical procedure was performed in the cathode channel. After the digitization, processing and storage stages, the system was armed again. The two resulting parameters were used to perform spectroscopy with depth sensing. The ratio of the anode and the cathode amplitudes is the depth index. The amplitude of the anode signal was histogrammed at different interaction depths. Once a spectra set was acquired at different detector slides, some correlation coefficients were obtained based on the photopeak centroid positions at different depths. Using these correction factors, a corrected global spectrum was collected at real time, together with the spectra at different depths and the raw total spectrum.

The effective dead time of the MPMCA was estimated with the *two-sources* method [10] by combining the ^{137}Cs source previously described with a ^{60}Co point source, 6300 Bq ± 4% activity, positioned in contact with the ^{137}Cs source. Results for a normalized live time of 1 h obtained from both acquisition methods are shown in Fig. 3a for non-correction configuration and in Fig. 3b for the case of corrected spectra. Fig. 3b shows that analog correction (anode relative gain adjustment) for the case of the spectrum acquired with the conventional MCA leads to rather similar results as those achieved with digital correction in the MPMCA (parametric correction of the amplitude as a function of depth). In any case, both corrected and uncorrected spectra comparison reveals that the MCMCA tool, in this source–detector geometry, is fully efficient and can be used

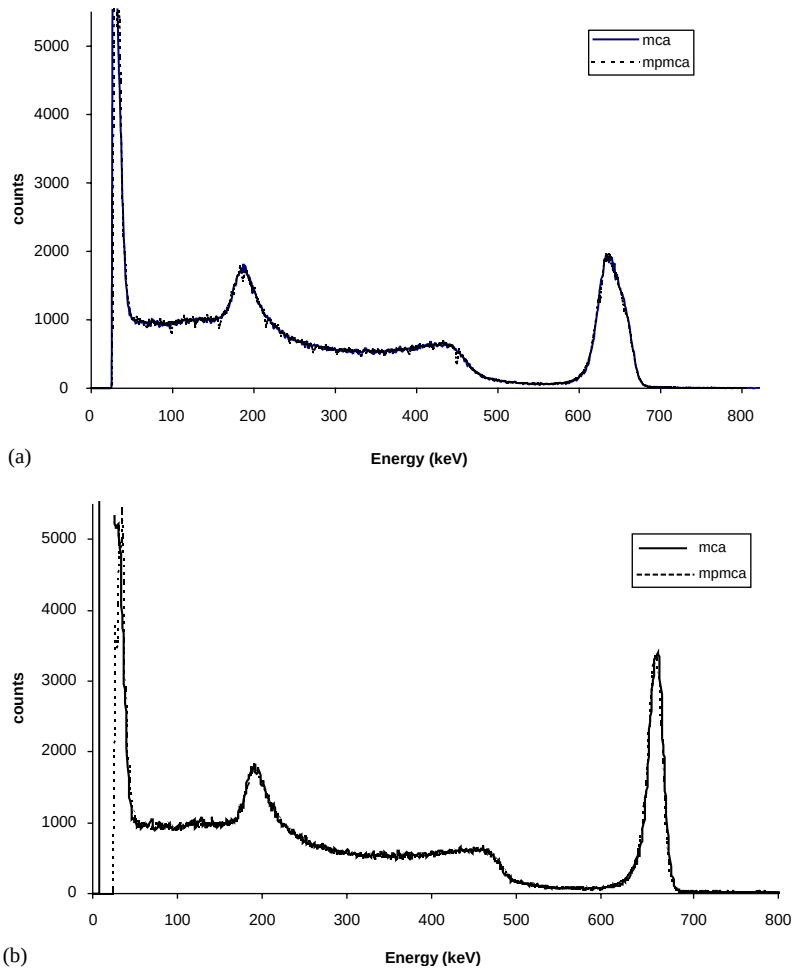

Fig. 3. Comparison of spectra acquired with the MCA and the MPMCA at identical geometric conditions and live acquisition time for a ^{137}Cs source. (a) No electron trapping corrections are considered. (b) Analog and digital corrections are considered in the MCA and MPMCA spectra, respectively.

for quantitative estimates of the detector efficiency.

3.2. Comparison with simulation

The simulated tool described above was used to check the experimental results. Only the region inside the last anode ring is considered as sensitive. Interactions outside this ring were disregarded. Two different simulations were performed:

(i) Simulation of the device as an ideal detector. The total amplitude for each single event is just the total energy deposited in the sensitive region of the crystal, with a random distortion in the pulse amplitude generated assuming a Gaussian distribution, in which the parameter σ is known from the experimental FWHM measured in MCA spectra at several energy positions using a precision test pulse generator (ORTEC 204). Values between 2.5% and 3.0% FWHM for the 662 keV peak were chosen in the simulations.

(ii) Basic approach to a coplanar detector. Eq. (1) was used to compute the deposited energy and was affected, in turn, by the electron trapping. A value of 6.5% for the proportion of electron

trapped per unit length was considered; this value was obtained from experimental results. The hole contribution was disregarded.

The results from the simulation (i) can be compared with the corrected experimental values, both MCA or MPMCA global spectra, whereas the results from simulation (ii) should be compared with uncorrected spectra. Comparison of these two simulations with experimental data are shown in Fig. 4.

In a second experiment, a lead collimator 2 cm thick, 2 cm diameter with a central aperture hole 1 mm diameter was positioned between the point source and the detector, centered in its axial direction, one face of the collimator in close contact to the point source, the other at 7 mm from the detector surface. It is obvious that the collimation effect for this radiation source is only partial; a much larger thickness would be needed to avoid the effect of low energy scattered photons in detector areas out of its central region. In any case, it represents a significant change in the

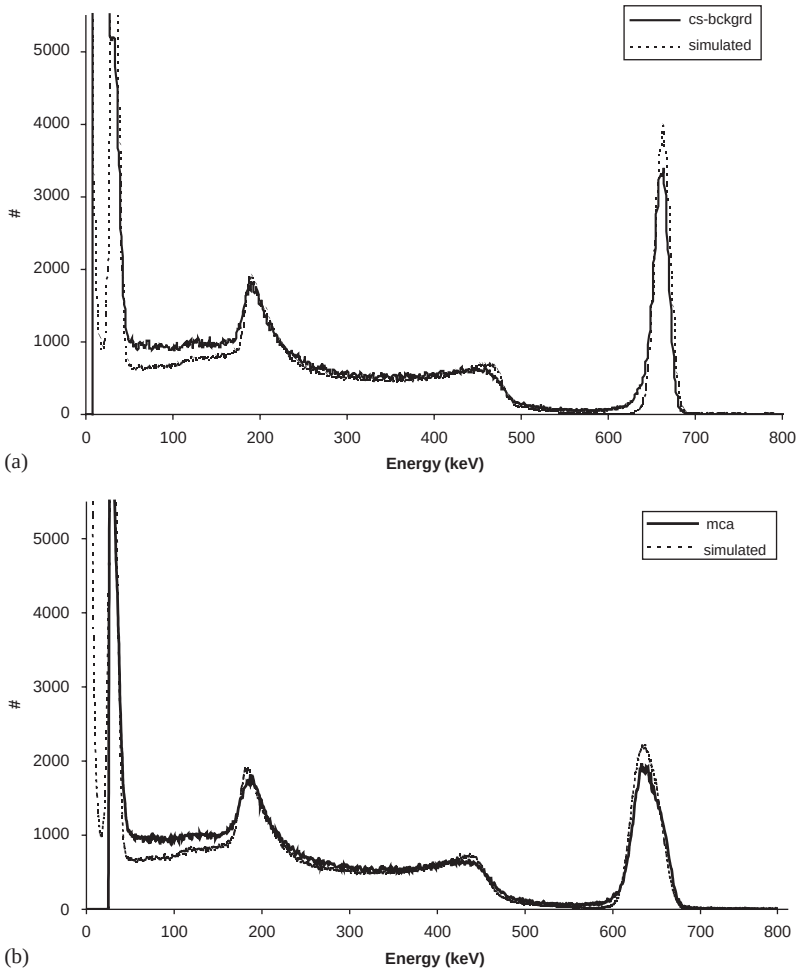

Fig. 4. Comparison of the simulated and experimental results obtained for corrected (a) and uncorrected (b) spectra, normalized to 1 h. Experimental spectra were acquired with the analog MCA. Simulation computed the ideal deposited energy affected by a gaussian fluctuation, such as described in the literature.

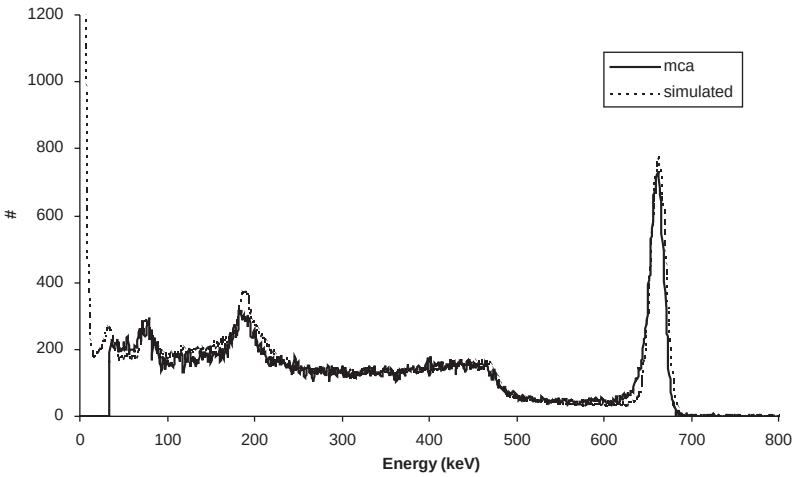

Fig. 5. Comparison of the simulated and experimental results similar to those show in Fig. 4b. This case considers a lead collimator 2 cm thick with a 1 mm diameter aperture hole, positioned in the detector axial axis.

Table 1
Relative comparison of simulated and experimental efficiency results for the CZT detector irradiated with a ^{137}Cs source

Relative differences in detector efficiency between simulation and experiment (experimental—simulated)			
Spectrum region	No collimator, uncorrected spectrum (%)	No collimator, corrected spectrum (%)	With collimator, corrected spectrum (%)
Total (50–800 keV)	8.4	8.4	−4.4
Compton (50–600 keV)	10.3	13.2	−4.0
Photopeak (600–700 keV)	−6.9	−9.9	−6.3

experimental setup geometry and can be useful for checking the simulation. Fig. 5 presents the comparison of experimental and simulated results, where the background was subtracted from the experimental spectrum. Comparing Fig. 5 with Fig. 4a, it can be seen that when the radiation is collimated, although only partially, towards the detector center, detector photopeak efficiency slightly improves and the low energy Compton region obtained in the experiment fits the simulated results better. This is an indication that gamma photons interacting in the external rings of the detector do not lead to a correct measurement of the deposited energy. This is expected for a coplanar detector; the region between the electrodes and the guard ring is sensitive, but induced charge is not proportional to the deposited energy.

Quantitative differences are summarized in Table 1. In this table, the experimental counting rate minus the simulated rates are shown relative to the simulated counting rate. The total, photopeak and Compton regions are also given in the table.

4. Depth sensing

4.1. Spectroscopy at different depths

Some collections of spectra discriminating interaction depth were acquired by using the MPMCA. The ratio between cathode and anode amplitudes (given by Eqs. (2) and (1), respectively, plus the Gaussian noise contribution) was used as interac-

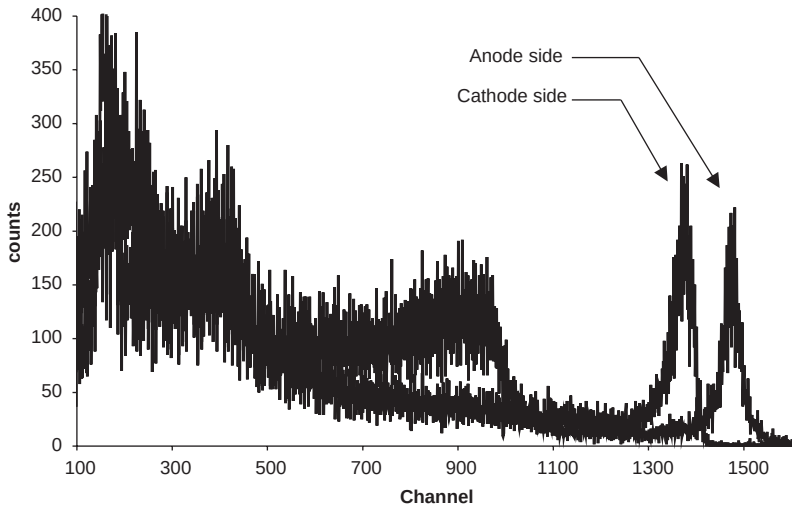

Fig. 6. Spectra acquired with the detector M02.2-1 and the MPMCA selecting interaction depths closer to anode and cathode faces. Acquisition (live) time: 60, 120 s.

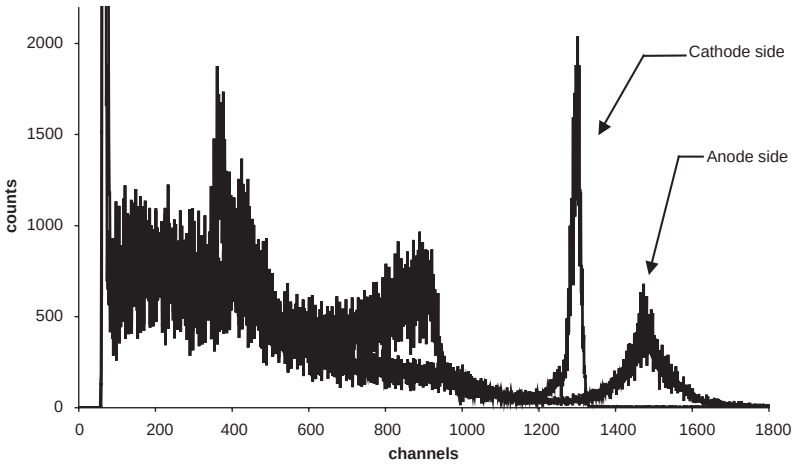

Fig. 7. Spectra acquired with the detector I9-04 (generation II) using a configuration identical to the one used in Fig. 6. Acquisition (live) time: 92,400 s.

tion depth coefficient such as described above. The amplitude of the anode pulses, shaped with a Gaussian amplifier, is used as an estimate of the energy. Fig. 6 shows the results obtained at the lowest and highest interaction depths values in which a significant spectrum was acquired. Two important results can be derived from the comparison of these two spectra. Firstly, although the photopeak shapes are rather different, the resolution of both photopeaks are comparable. In this detector, the reported phenomena of resolution degradation at interaction depths closer to the anode side was not observed. This is a direct consequence of the anode pattern design. Thus, Fig. 6 is evidence of the correct balancing of the anode weighting potentials. Secondly, as expected, the photopeak position decreases as the depth coefficient rises from 0.0 (anode side) up to 1.0 (cathode side). This effect is associated with trapping under gone by the electrons in their drifts towards anode face. The surprising result is the relative low difference in the peak positions, below

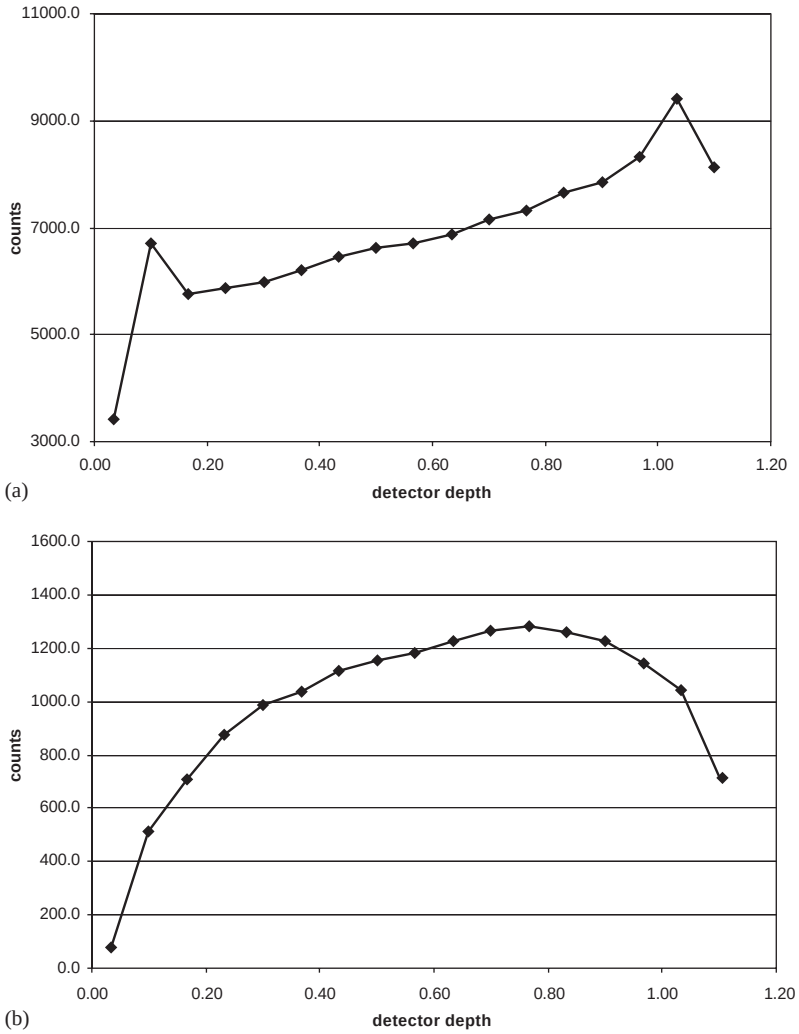

Fig. 8. Total (a) and photopeak (b) efficiency obtained with the MPMCA at different interaction depths normalized for an acquisition live time of 1 h.

6.7%, whereas a value ~10% is normally reported for similar devices. This value was used in the simulation as input parameter.

In order to confirm the conclusions outlined above, similar measurements were performed with the same setup using a detector with anode pattern of a previous generation (generation II [4]), the I9-04 unit, manufactured by eV-Products. Spectroscopic results for the same interaction depths shown in Fig. 6 are given in Fig. 7 for this detector. The geometry and electronic setup was identical to the one used for Fig. 6 except that the acquisition time was different. The improvement of the new detector regarding spectroscopic resolution homogeneity throughout the crystal depth is evident. Moreover, the difference in the peak position leads to an electron trapping rate ~11% in this case.

A comparison of Figs. 6 and 7 provides hints about why the overall energy resolution from detector M02.2-1 is lower than from detector I9-04, in spite of the good resolution homogeneity

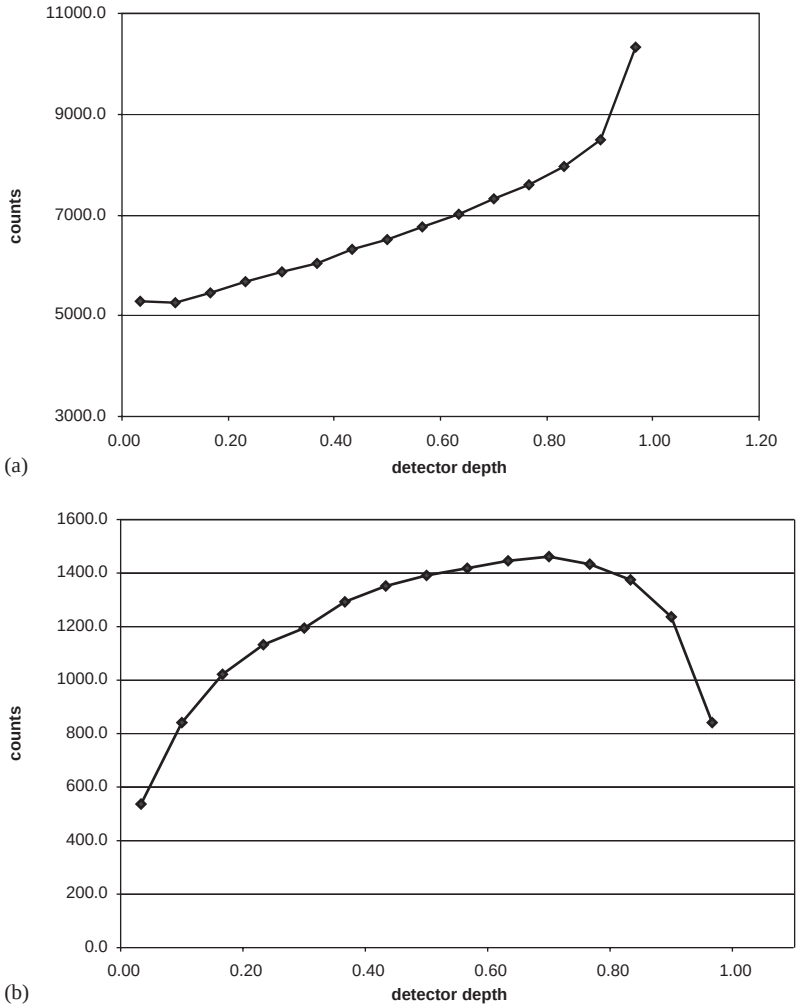

Fig. 9. Total (a) and photopeak (b) efficiency obtained from the simulation of the experimental setup used in Fig. 8.

achieved at different interaction depths. The spectrum obtained for interactions near the cathode from detector I9-04 indicates the best spectroscopic resolution achievable in this detector, which is significantly better than the one obtained from detector M02.2-1 in the same region. The resolution of the I9-04 detector is poorer because of the contribution of the regions near the anode face. In detector M02.2-1, the lower resolution is not due to flaws in the electrode balancing, but due to global effects in the device.

4.2. Detector efficiency

Regarding detector efficiency at different depths, Fig. 8 presents total (Fig. 8a) and photopeak (Fig. 8b) counting rate obtained at different interaction depths. These data can be compared with those obtained from the simulation, Fig. 9. Both results are normalized to an acquisition time of 1 h. The values of efficiency integrated for all the interaction depths agree in both cases according to the terms quantified in Table 1. Qualitative similarity of efficiency trends

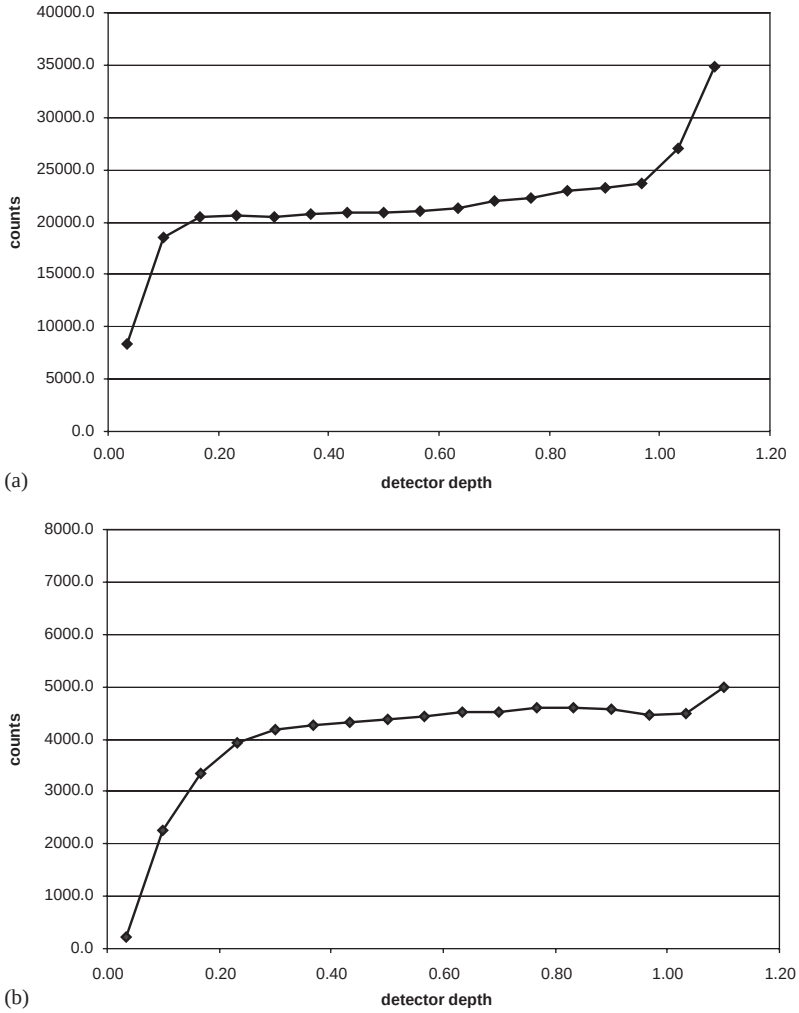

Fig. 10. Total (a) and photopeak (b) efficiency obtained with the MPMCA for the detector I9-04 at different interaction depths normalized for an acquisition live time of 1 h.

versus interaction depth is observed. These were only affected by three facts:

(i) The maximum value obtained experimentally for the ratio between cathode and anode pulse amplitudes is larger than 1.0, as can be seen in Fig. 8. A probable contribution to this problem may be related to differences in the anode and cathode channel gains. In spite of the care taken to adjust these gains, factors out of our scope and control still affected the results significantly.

(ii) Results of the simulation for total efficiency reveals that the detected number of counts in the detector region closer to electrodes is not accurate.

(iii) Results of the simulation for photopeak efficiency over estimate the detector efficiency in the region closer to the anode side.

It is worth comparing the experimental results obtained with the two detectors M02.2-1 and I9-04. Fig. 10 shows results obtained from detector

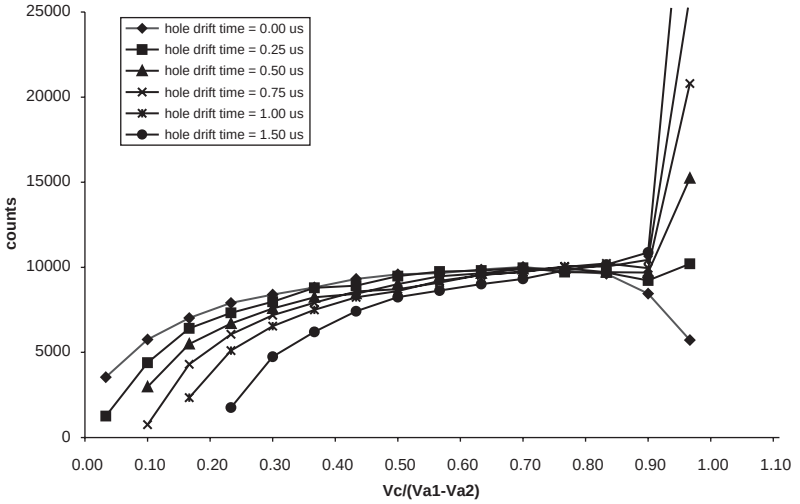

Fig. 11. Photopeak efficiency obtained from the simulation of the experiment in Fig. 8 assuming hole contribution in the cathode signal for different values of maximum permitted drift time.

I9-04. The response of detector M02.2-1 is closer to that theoretically expected than detector I9-04.

4.3. Effect of hole contribution

In this section the effects of the charge induced by holes was disregarded. Although marginal, the drift of holes can have an influence on the detector efficiency at different depths. In order to study how the charge induced by holes can affect the detector efficiency, Eqs. (3) and (4) were used in the simulation for the cathode signal amplitude. As mentioned previously, since we are using the coplanar anode signal collection technique [5], it is assumed that the anode signal is completely insensitive to hole drift.

A set of simulations were run taking into consideration different values of the maximum permitted drift time for holes. Some of the results are shown in Fig. 11, where the photopeak efficiency is plotted against the estimated interaction depth. The general trend is that the higher the maximum permitted hole drift time, the higher the number of counts in the last detector slice (near cathode) and the lower the number of counts in the anode side. For hole drift times in the order of 0.5 μs, no counts were found in the first of 15 slices close to the anode face. Results comparable with the experiment were found for 0.25 μs maximum permitted hole drift time. This result is given in Fig. 12.

Fig. 12 shows how the trend of reducing photopeak efficiency in the region closer to anode face can be explained by making use of the hole contribution. On the other hand, the general trend of the total efficiency of the experimental detector (Figs. 8a and 12a) is also compatible with that shown in Fig. 12a.

5. Discussion

This study presents some experimental and simulated results obtained from a large CZT coplanar detector. From the comparison between a Monte Carlo simulation and the experiment, it can be concluded that a basic coplanar model is sufficient to understand the efficiency of the detector presented here. This holds for both its total volume and at different interaction depths between cathode and anode. The implemented model was based on the amplitudes of pulses induced by the radiation on the collecting anode, non-collecting anode and cathode for ideal coplanar devices. Total and photopeak experimental efficiencies fit the expected results with errors

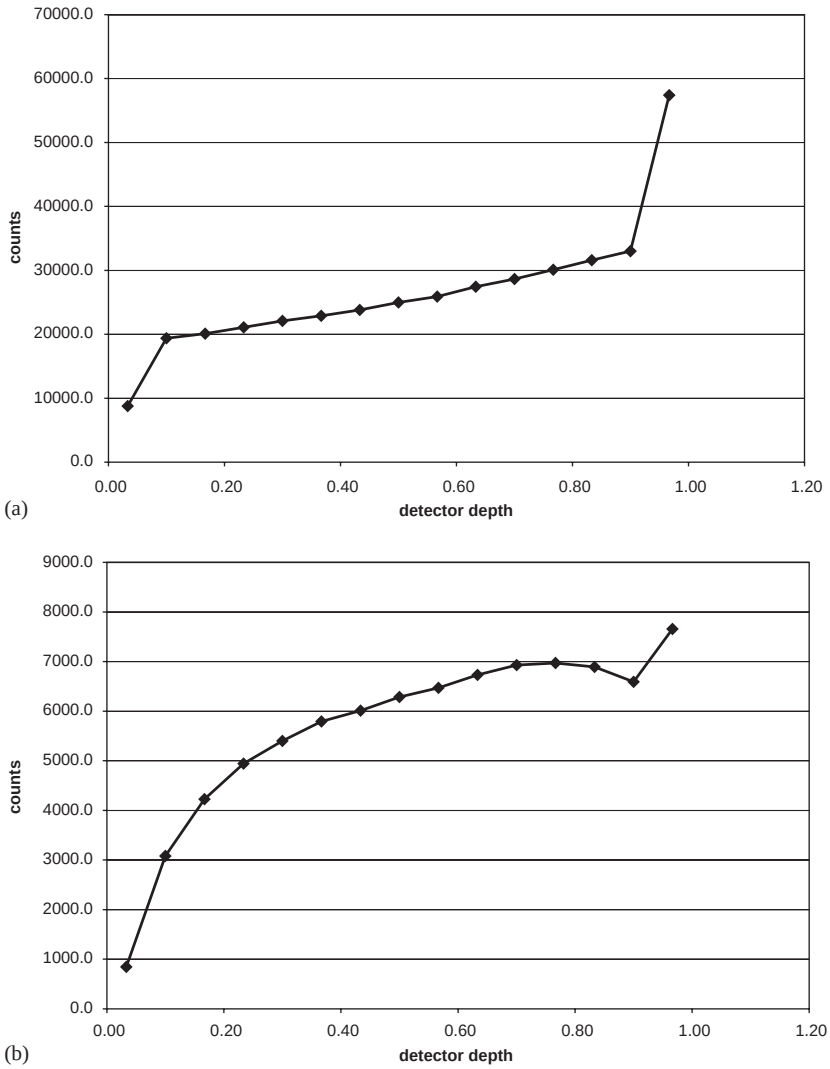

Fig. 12. Total (a) and photopeak (b) efficiency obtained from the simulation of the experiment in Fig. 8 assuming hole contribution in the cathode signal for 0.25 μs maximum permitted hole drift time.

below 10%. Interaction depths profiles obtained in these experiments are similar to those expected, in clear contrast with other previously used similar devices. Errors on the interaction depth scaling have been detected.

Spectroscopic results at different interaction depths reveal that the anode design in this detector leads to an acceptable weighting potential balance. In practice, the spectroscopic resolution does not depend on the interaction depth. From the photopeak positions at different interaction depths the electron trapping rate in the crystal can be estimated to be $\sim 6.5\%$, a low value if compared with similar detectors.

Regarding detector drawbacks, total counting rate at regions near the electrode were considered not to be accurate. The method for estimating the interaction depth used in this work leads to uncertainties in these two regions. We show that residual hole contribution in the cathode signal

can minimize the over estimate of photopeak efficiency in the region near the anode face given by the simulation when only negative charge is taken into account. Since this is not the only explanation for this effect, further studies have to be carried out in order to experimentally quantify the effective maximum drift time of holes and the thickness of the layer near anode in which holes drift towards non-collecting anode.

The major limitation observed in the detector is related to the relative poor resolution in all interaction depths, particularly in the region of the crystal near the cathode face, where the best resolution should be expected. According to information provided by the vendor, there is a clear difference between the I9-04 (generation II) detector and the one used in this study. The crystal in detector M02.2 was grown by eV Products in a new generation furnace. These furnaces have a much higher yield in the production of large single crystals and grow material with higher $\mu\tau$ product of electrons. However, they currently have more and larger Te inclusions [11] (30–50 μm in size). This means that the fluctuation of electron generation and trapping is large, resulting in poorer energy resolution. However, current measurements are being carried out in order to quantify this effect.

Finally, in the code presented in this paper, the Shockley–Ramo theorem is considered just for estimating the maximum pulse amplitudes in ideal detectors, disregarding the particular pulse profiles associated with the anode pattern in the coplanar detectors. Obviously, this is a simplification that leads to errors in the estimate of interaction depth profiles. To overcome this limitation, the authors are working on a new version of the code in which the electric field and weighting potentials in the coplanar detectors presented in this work will be included, starting with the electrostatic case. The charge generated by the radiation will be drifted towards the electrode within a simulated electric field, thus providing a better approach to the induced charge in cathode and anodes.

Acknowledgements

This work was supported by the Spanish Ministry of Science and Technology, under the research project ref. TIC2002-02367.

References

[1] J.M. Pérez, Z. He, D. Wehe, IEEE Trans. Nucl. Sci. NS-48 (3) (2001) 272.
[2] J.M. Pérez, Z. He, D.K. Wehe, Y.F. Du, Estimate of large CZT detector absolute efficiency, IEEE Nuclear Science, August 2002, Vol. 49, no.4, pp. 2010–2018.
[3] P.N. Luke, M. Amman, J.S. Lee, B.A. Ludewight, H. Yaver, Nucl. Instr. Meth. A 458 (2001) 319.
[4] P.N. Luke, Appl. Phys. Lett. 65 (22) (1994) 2884.
[5] P.N. Luke, IEEE Trans. Nucl. Sci. NS-42 (4) (1995) 207.
[6] Z. He, G.K. Knoll, D.K. Wehe, Y.F. Du, Nucl. Instr. and Meth. A 411 (1998) 107.
[7] Z. He, G.K. Knoll, D.K. Wehe, R. Rojeski, C.H. Mastrangelo, M. Hamming, C. Barret, A. Uritani, Nucl. Instr. and Meth. A 380 (1996) 228.
[8] S. Agostinelli, et al., Nucl. Instr. and Meth. A 506 (2003) 250.
[9] Z. He, Nucl. Instr. and Meth. A 463 (2001) 250.
[10] G.F. Knoll, Radiation Detection and Measurement, 3rd Edition, Wiley, New York, 2000.
[11] M. Amman, J.S. Lee, P.N. Luke, J. Appl. Phys. 92 (6) (2002) 3198.